Snapshot Tracking of GNSS Signals in Space: A Case Study at Lunar Distances

Snapshot Tracking of GNSS Signals in Space: A Case Study at Lunar Distances

Andrea Nardin, Alex Minetto, *Politecnico di Torino, Turin, Italy*
Salvatore Guzzi, *Qascom s.r.l., Bassano del Grappa, Italy*
Fabio Dovis, *Politecnico di Torino, Turin, Italy*
Lauren Konitzer, Joel J. K. Parker, *Goddard Space Flight Center (GSFC), NASA, Greenbelt, (MD), USA*

BIOGRAPHY

Andrea Nardin received the M.Sc. degree in Telecommunications engineering and the Ph.D. degree in Electrical, Electronics and Communications Engineering, in 2018 and 2023, respectively, both from Politecnico di Torino, where he is currently a postdoctoral researcher. From 2018, he has been working on satellite navigation technologies with the Navigation Signal Analysis and Simulation (NavSAS) group at Politecnico di Torino and in 2021 he was a Visiting Doctoral Researcher at Northeastern University, Boston, MA, USA with the Information Processing Lab (IPL).

Alex Minetto received the B.Sc. and M.sc. degrees in Telecommunications Engineering from Politecnico di Torino, Turin, Italy and his Ph.D. degree in Electrical, Electronics and Communications Engineering, in 2020. He joined the Department of Electronics and Telecommunications of Politecnico di Torino in 2021 as researcher and assistant professor. His current research interests cover navigation signal design and processing, advanced Bayesian estimation applied to Positioning and Navigation Technologies (PNT) and applied Global Navigation Satellite System (GNSS) to space weather and space PNT.

Salvatore Guzzi received the M.Sc. degree in Communications and Computer Networks engineering in 2022 from Politecnico di Torino, with a thesis on the study of high sensitivity GNSS receivers for space applications and lunar missions, carried out with the Navigation Signal Analysis and Simulation (NavSAS) group. He is currently working as a Software Defined Radio Engineer at Qascom, Bassano del Grappa, Italy, focusing on high sensitivity and robust GNSS processing for harsh environments.

Fabio Dovis received his M.Sc. degree in 1996 and his Ph.D. degree in 2000, both from Politecnico di Torino, Turin, Italy. He joined the Department of Electronics and Telecommunications of Politecnico di Torino as an assistant professor in 2004 and as associate professor in 2014. Since 2021 he is a full professor. He coordinates the Navigation Signal Analysis and Simulation (NavSAS) research group. His research interests cover the design of GPS and Galileo receivers, advanced signal processing for interference and multipath detection and mitigation, as well as ionospheric monitoring.

Lauren Konitzer received an M.S. in Aerospace Engineering and Mechanics from the University of Minnesota - Twin Cities in 2019. She is a navigation and mission design engineer at NASA Goddard Space Flight Center. She is the Deputy Principal Investigator for the Lunar GNSS Receiver Experiment (LuGRE), and is a flight dynamics analyst for the Roman Space Telescope.

Joel J. K. Parker is the PNT Policy Lead at NASA Goddard Space Flight Center where he is involved in national and international projects related to GNSS and space-based PNT services. He co-chairs the Space Use Subgroup of the International Committee on GNSS and is the PI for the Lunar GNSS Receiver Experiment (LuGRE) payload on the Firefly Blue Ghost Mission 1, landing on the lunar surface in 2024.

ABSTRACT

The latest space missions have unveiled GNSS usability for distances greater than 187 000 km from the Earth's surface. The actual availability and usability of GNSS signals beyond such an altitude are still questionable, and experimental evidence still lacks. The Lunar GNSS Receiver Experiment (LuGRE) is a joint NASA-Italian Space Agency (ASI) payload aiming at demonstrating GNSS-based positioning, navigation, and timing through its trajectory towards the Moon. After the launch in 2024, the payload will receive multi-frequency Global Positioning System (GPS) and Galileo signals across the different mission phases, and will conduct onboard and ground-based scientific experiments. Besides positioning and raw GNSS observables, the LuGRE payload will deliver snapshots of GNSS digital signal samples. Such snapshots will be at the core of a set of science investigations, and require the development of a post-processing unit being operated within the LuGRE ground segment throughout the mission. In this paper, we present an analysis that aims at identifying a minimum snapshot duration suitable for a successful, post-processing tracking of the recorded signal along the Moon transfer orbit and on the Moon surface. The processing of realistic mission-related signals has been performed to tune the receiver architecture and investigate the tracking performance in the LuGRE framework. Subsequently, a statistical analysis of the tracking lock conditions has been carried out leveraging a Monte Carlo approach to characterize the performance for different settings of the receiver front-end.

I. INTRODUCTION

Navigation in space is a wide application field where the race for improving accuracy, reliability and autonomy involves different areas of expertise. The use of inertial systems (i.e., gyroscopes) and star-trackers is ubiquitous in space missions, but the error of their fused navigation solutions may significantly drift over time unless frequent and accurate external updates are provided. Spacecraft generally rely on hybrid navigation/communication links to a global network of ground tracking stations, originated by the National Aeronautics and Space Administration (NASA) with the Deep Space Network (DSN), and followed by the European Space Agency (ESA) and the Japan Aerospace Exploration Agency (JAXA) with the European Space Tracking (ESTRACK) network and the Tracking and Communication Center, respectively. Such networks allow operators to estimate the spacecraft's state thanks to radiometric measurements such as range, Doppler frequency, and very-long-baseline interferometry (VLBI) (Thornton and Border, 2003). These consolidated techniques can ensure an accuracy down to tens of meters for deep space missions (Thornton and Border, 2003). Nevertheless, they present some limitations. Firstly, the navigation process cannot be performed real-time, thus it is not usable for critical operations. Secondly, the spacecraft navigation process ultimately happens on the ground rather than onboard, constantly relying on the ground segment and therefore losing autonomy, a long-time issue for space assets (Nardin et al., 2022a). Alternatively, the state estimation can be performed through onboard autonomous navigation. Different technologies were implemented in this direction such as celestial navigation via the use of optical techniques, and X-ray pulsar navigation (Franzese et al., 2018; Xiaolin et al., 2018).

Although Global Navigation Satellite Systems (GNSSs) were originally designed to provide positioning, navigation, and timing (PNT) for terrestrial users, the benefits to extending their use to the space service volume (SSV) (ISECG, 2018) and beyond are several. Indeed, they will (*i*) enable autonomous navigation in real-time. Spacecraft can obtain PNT information which is critical to mission operations, allowing them to react and respond to unforeseen events in real-time and ensuring safety of the mission. GNSS receivers can also simplify ground operations, thus (*ii*) reducing the need for tracking facilities and overall operational costs. Furthermore, GNSS precise time estimation capability can also be used as a (*iii*) timing source for hosted payloads or to enable cooperative navigation paradigms requiring accurate time sync among the nodes (Delépaut et al., 2022). In general, GNSS accuracy can help missions to get reliable measurements from space, hence (*iv*) enable a large number of scientific opportunities (Baird, 2021). However, besides advantages (*i-iv*), the use of GNSSs signals above the GNSS constellations presents critical aspects that must be taken into account. Extremely low power levels caused by Earth's umbra and long distances (Baird, 2021; Winternitz et al., 2017) lead to (*i*) weak GNSS signal power and (*ii*) limited satellites' visibility. Moreover, the high receiver altitude is characterised by (*iii*) poor satellites geometry, i.e., high dilution of precision (DOP), which translates to low-precision of navigation solutions. High spacecraft speed might be responsible for (*iv*) higher values of Doppler shift when relative velocities between the satellite and the receiver are large. GNSS signal tracking in these conditions is generally more difficult and time consuming compared to terrestrial applications. To mitigate such critical aspects, signals coming from different constellations and transmitted on different bands can be exploited concurrently by multi-constellation, multi-frequency receivers. Furthermore, the use of adequate antenna and advanced signal processing techniques can effectively contribute to the reception of weak GNSS signal (Dovis and Ta, 2012). Despite critical aspects (*i-iv*), GNSS is dominant on many levels such as autonomy, accuracy, and cost with respect to other relevant techniques (Thornton and Border, 2003; Franzese et al., 2018; Xiaolin et al., 2018). Indeed autonomous Global Positioning System (GPS) navigation at very high altitudes has been already demonstrated by NASA's Magnetspheric Multiscale (MMS) mission at 187 167 km (Winternitz et al., 2017; Baird, 2019). This justifies the escalating interest to test and extend GNSS receivers to the Moon and beyond. However, the use of GNSS at higher altitudes is an unexplored field and even if the recent studies are encouraging, still no guarantees are present. Despite the elevated prospects, some questions remain open on the feasibility, but a new era of lunar exploration makes GNSS usability in space strongly attractive.

Current lunar exploration efforts involve more than eighty national space agencies and several private companies and partnership, making the Moon again a top space exploration priority (ISECG, 2018). NASA and other space agencies look at the GNSS as a crucial enabling technology for cislunar and lunar navigation, particularly in the near future (Delépaut et al., 2020). NASA and ESA have published plans for lunar communications and navigation infrastructures that will provide one-way radionavigation signals in lunar orbit, addressing the visibility, geometry, and signal-strength limitations of using solely Earth-based GNSS (Israel et al., 2020). A phased approach is required to develop both capabilities and transition between them. The Lunar GNSS Receiver Experiment (LuGRE) will support the first step of this strategy, demonstrating the feasibility of using GNSS for lunar navigation (Parker et al., 2022; Nardin et al., 2022b; Minetto et al., 2022).

LuGRE is a joint NASA-Italian Space Agency (ASI) payload on the Firefly Blue Ghost Mission 1 lander, selected by the Commercial Lander Payload Services (CLPS) program to demonstrate GNSS-based positioning, navigation, and timing at the Moon. After the launch in 2024, the payload will receive multi-frequency GPS and Galileo signals across the different mission phases, and will conduct onboard and ground-based scientific experiments.

These investigations will be based on the observation of the data collected by a custom development performed by the company Qascom, based on the Qascom QN400-Space GNSS receiver. The receiver is made of two core modules: a baseband processor implemented through software-defined radio (SDR) technologies and a radio frequency (RF) front-end. The receiver computes

multi-frequency, multi-constellation state estimates, and provides the GNSS raw observables obtained by the real-time operation, as well as snapshots of intermediate frequency (IF) digital samples collected by the RF front-end at frequencies L1 and L5 for GPS and E1 and E5a for Galileo. These data will be the input for a set of scientific investigations. The current work done by the science team of NASA and ASI, which is supported by a research team at Politecnico di Torino, is planning the data acquisitions during the time windows dedicated to the LuGRE payload in the checkout, transit, and surface mission phases.

Besides conventional GNSS data, the availability of IF samples on the ground will allow the team to (*i*) record and replicate the remote scenario, and (*ii*) perform additional advanced signal processing not available in real-time. Signal sample datasets will turn the probe into a test-bed for future acquisition/tracking engine research for autonomous GNSS in space. All the LuGRE science data will be released to a public archive for the benefit of the navigation and space communities.

Due to mission constraints (Parker et al., 2022), the collection and downlink windows of IF signal samples will be limited to spans of few hundreds of milliseconds. Given a fixed datarate and downlink window duration, the available time length of the digital signal chunk ultimately depends on the sampling frequency and quantization depth. A consolidated branch in GNSS, known as snapshot positioning, addresses the processing of such short snapshots of signal samples to infer the receiver location, also without a-priori information (Fernández-Hernández and Borre, 2016). A portion of the scientific investigations foreseen by the LuGRE project utilize this paradigm to inform future space applications.

The purpose of this work is then twofold. On the one hand, achievable tracking performance in post-processing is tested, in contrast to the operational acquisition and tracking that LuGRE will perform in other data-collection modes throughout the mission, relying on a time-limited record data of GNSS signals. Simulated radio frequency (RF) signals, as received along the mission trajectory through the LuGRE receiver, are post-processed with a high-sensitivity software GNSS receiver, that leverages the snapshot positioning paradigm to achieve a successful signal tracking with very limited stretches of samples. On the other hand, the impact of sampling frequency and number of quantization bits on the time needed to get to signal tracking lock is investigated. This information can drive the duration of the snapshot and can be used to effectively design and schedule the baseband data collection process that will be performed by the LuGRE receiver throughout the mission. The next section provides an overview of GNSS receiver stages, successful signal tracking definition, and weak signal tracking conditions. Data generation, receiver settings, and Monte Carlo setup are described in Section III while results are presented and discussed in Section IV. Conclusions are drawn in Section V.

II. BACKGROUND

1. The GNSS Receiver

The main task of the GNSS receiver is to measure the propagation time of the navigation signal with high precision. The operations that it executes are to receive, amplify, and filter GNSS signals transmitted by satellites and apply analog-to-digital conversion; to separate the different channels and generate local code replicas to demodulate the signal; to estimate the GNSS signal code phase for pseudorange measurement and carrier phase for carrier phase measurement; to demodulate the navigation message and eventually solve for the position, velocity and time (PVT) equations (Spilker Jr et al., 1996). The mentioned operations can be grouped in five functional blocks composing a typical receiver architecture that are known as (*i*) *front-end* stage; (*ii*) *acquisition* stage; (*iii*) *tracking* stage; (*iv*) data demodulation; and (*v*) PVT engine. The acquisition stage reveals which satellites are in radio visibility and performs a coarse estimate of their Doppler frequency and code phase. Subsequently, such estimates are given as input to the tracking stage to initialize the local code and carrier generation blocks, shown in Figure 1. Within the tracking loops, both the code phase and the Doppler frequency are refined. These estimates are used to build the so-called *pseudoranges*, *Doppler* and *carrier-phase* measurements between the receiver and the satellites. The latter are used as input measurements for the estimation of the PVT. Acquisition and tracking must run continuously in parallel, since the satellites are moving permanently, appearing and disappearing over time. Figure 1 illustrates a simplified block diagram of a tracking stage, in which two main loops—highlighted in dashed boxes—are in charge of the generation of code and carrier local replicas.

The presence of two codependent loops in the tracking architecture makes a performance analysis typically difficult, and a closed mathematical form to describe the convergence of the system is not fully understood (Teunissen and Montenbruck, 2017). The tracking stage converges to the best solution of the parameters only if the initialisation values provided by the acquisition stage are sufficiently accurate. If the tracking converges to a solution, it is said to be *locked* meaning that a stable solution of the double loop is found. The carrier tracking loop is a feedback loop able to finely estimate the frequency and the phase of a noisy sinusoidal waveform and to track the frequency changes while the satellite and the receiver are moving. It is defined by the carrier loop discriminators which act on the outputs of correlators and can be implemented through a phase-locked loop (PLL) and possibly a frequency-locked loop (FLL), which might be used to initialize the carrier numerically-controlled oscillator (NCO) (see Figure 1). An FLL tracks the Doppler frequency completely ignoring the carrier phase. It is more robust against dynamic stress, but is less accurate than a PLL (Teunissen and Montenbruck, 2017). To take advantage of both, an FLL-assisted PLL can be used (Yang et al., 2017). This branch of the tracking can be viewed as a chained code wipe-off and carrier tracking,

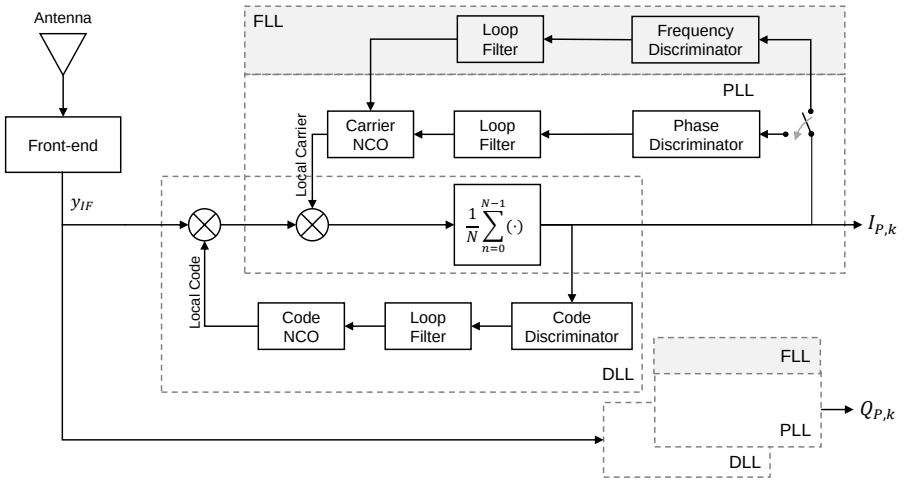

Figure 1: High-level block diagram of a tracking stage, derived from (Borio and Gioia, 2023). Dashed boxes highlight local code and carrier generation loops, N identifies the amount of signal samples considered within the k-th integration loop.

since prior to the carrier tracking, the spreading code should be removed from the signal. Conversely, when estimating the delay, the carrier frequency has to be removed. The carrier wipe off is performed by multiplying the signal by a sinusoidal signal generated by a local oscillator, in principle perfectly locked to the incoming carrier thanks to the estimate of the Doppler shift and the carrier phase. The result of this operation is a baseband signal from which information on the delay can be retrieved. The code tracking loop is then performed by means of a delay-locked loop (DLL).

2. The phase lock indicator and the time to lock

On the basis of error information, tracking convergence can be defined. In other words, if the tracking error is lower than a specific threshold, then the system will converge. When the convergence of the double loop is achieved, the tracking is locked, indicating that the signals' parameters are accurately estimated and tracked by the system. However, due to the presence of the double loop, the tracking architecture is complex and a closed form to define the convergence of the system does not exist. Some indicators, referred to as *lock detectors*, can be used to accomplish the presented task. One of these is named phase lock indicator (PLI) (Spilker Jr et al., 1996). The PLI is computed by means of the prompt I and Q correlator outputs of the carrier tracking algorithm, such that

$$PLI_k = \frac{I_{P,k}^2 - Q_{P,k}^2}{I_{P,k}^2 + Q_{P,k}^2} \approx \cos\left(2\delta\varphi_k\right) \quad \text{where} \quad \delta\varphi_k = \arctan\left(\frac{Q_{P,k}}{I_{P,k}}\right) \tag{1}$$

is the phase error and $I_{P,k}$, $Q_{P,k}$ are the prompt correlator outputs for the in-phase (I) and quadrature-phase (Q) signal components, respectively, computed at the k-th integration loop. The more the PLI is near to the ideal value, the lower is the phase error at the output of the PLL. The PLI concept can be exemplified for Galileo E1C signal: if the loop is in phase lock, then $I_{P,k}$ will be close to the maximum attainable correlation value over the integration time while $Q_{P,k}$ will be around zero (Teunissen and Montenbruck, 2017; Kaplan and Hegarty, 2017). In this ideal situation the value of the PLI is expected to be 1. In practice, to implement a phase lock detector, a threshold is taken into account. Setting a threshold on the PLI_k value means fixing a tolerance for the phase error. The higher the value of the threshold, the lower the phase error permitted, and hence the lock declaration will be more reliable. However, having a high threshold means also increasing the probability to not declare a lock when this happens (false negative), especially at low Carrier-to-Noise-density ratio (C/N_0). If at a given k, PLI_k is lower than the threshold, then this is indicated as a point of tracking loss (Savas et al., 2021). Different algorithms can be employed to declare the lock based on the loss of tracking points (Kaplan and Hegarty, 2017). The simplest one is the decision logic based on hard thresholding of the PLI value. When PLI_k exceeds the value of the threshold for the first time, the lock is achieved. Such a decision logic is poorly reliable in case of low C/N_0. In this case, more robust algorithms can be adopted, allowing to reduce the false lock declaration probability (Kaplan and Hegarty, 2017). In this work, an approach based on the use of subsequent PLI values above threshold is considered, to take advantage of a more robust decision logic. The amount of subsequent values as well as the threshold should be set depending on the specific environmental and operational conditions of the receiver. The implementation details will be given in Section III.2.

3. Weak GNSS signal tracking techniques

Several tracking issues may arise if the environment is degraded as in case of high altitude. Large Doppler and low C/N_0 conditions to mention a few. For these reasons, the tracking needs to be made more robust against the noise and more sensitive to face high relative dynamics. To this purpose, the tracking parameters can be designed and modified to operate on this scenario and different tracking architectures can be considered if needed. The proper design of the parameters is a challenging task since many trade-offs occurs. A GNSS receiver should have a short *integration time*, an FLL discriminator and a wide filter bandwidth to tolerate dynamic stress. Conversely, it should have a large integration time, a PLL discriminator and a narrow bandwidth to be robust against the noise and more accurate. The integration time is the time over which the loop correlators are integrated and it is strictly related to the loop bandwidth. It involves a trade-off since it should be extended as much as possible to operate under weak signal conditions, but a short integration time is needed to operate under high dynamic stress. This is less problematic if good C/N_0 conditions are met, even under intense Doppler (Nardin et al., 2020, 2021). However, in a harsh environment such as space, both dynamics and low C/N_0 may be experienced. Therefore, changing the parameters could be not enough to successfully track the signal. Alternative tracking architectures and external aiding are then considered to this purpose. As an example, the use of an adaptive orbital filter (OF) to aid the acquisition and the tracking of very weak signals was demonstrated to lead to a higher accuracy on the navigation solutions. The impact of employing an orbital filter on the acquisition and tracking was shown in other studies (Capuano et al., 2016)(Musumeci et al., 2016a)(Capuano, 2015)(Silva et al., 2013). They all argue that the OF is gainful and profitable for the GNSS receiver for space applications

III. METHODOLOGY

1. Simulated Data Generation

Two datasets are used in the proposed analysis. Both are made of digitized IF samples of the in-phase and quadrature components of a simulated received signal, generally referred to as I-Q samples (IQS). The first IQS set emulates GNSS signals received at four different points spanning the LuGRE mission trajectory, corresponding to 30 RE, 45 RE, 60 RE, and 61 RE. To provide a perspective on the investigated space volume, it is worth remarking that 1 RE $\simeq 6371$ km is the mean Earth radius and 60.4 RE is the Earth-Moon mean distance (Williams and Dickey, 2002). Such a set is the result of a RF GNSS signal simulator fed with the mission trajectory and connected to the front-end of the LuGRE receiver. Signals are then collected at the output of the front-end, after analog-to-digital conversion. The specifics of what will be called the *simulated RF samples* are reported in Table 1. The GNSS L1 band—including GPS L1 C/A and Galileo E1 signals—is considered in this analysis. The second dataset

Table 1: The specifics of simulated RF samples at L1 band

Parameter	30 RE	45 RE	60 RE	61 RE
Sampling freq. (Msps)	8	8	8	8
Quantization bits (bits)	8	8	8	8
Duration (ms)	400	1000	1000	1000
Snapshots	1	2	4	1

is simulated using FUll Educational Library of Signals for Navigation (N-FUELS), a software-based GNSS digital baseband signal generator (Falletti et al., 2013). N-FUELS is a signals and disturbances simulator that has been implemented as a set of non-realtime MATLAB functions. It is able to simulate the GNSS signal samples seen at the receiver after the analog-to-digital conversion of the incoming analog signal. The use of *N-FUELS samples* enables a more in-depth analysis on the tracking performances thanks to the capability of replicating and generating the signals under a variety of conditions. Following this, the LuGRE scenario has been simulated by setting the expected C/N_0 levels and Doppler profile at the different points along the mission trajectory. A previous worst-case analysis on the acquisition performance (Nardin et al., 2022b) considered C/N_0 values corresponding to transmitting antenna side lobes. To reduce the possibility of unreliable results on the tracking performance, the current investigation addresses a more conservative antenna pattern where only main lobes are modelled. The simulated values at 45 RE were 30 dB-Hz and 31 dB-Hz for GPS and Galileo, respectively. At 60 RE, they were instead set to 27 dB-Hz and 28 dB-Hz. All the signals were processed by means of the NavSAS software GNSS receiver.

2. Software Receiver Tuning

The tracking stage must be thoroughly configured to effectively cope with the space scenario. Parameter tuning was done through a set of preliminary analyses, the results of which are reported in Section IV.1. The same approach was used for the acquisition settings along with the findings of a previous study (Nardin et al., 2022b). A preliminary analysis of the simulated RF samples revealed that we are not able to acquire any satellite by following the conventional acquisition procedure. Strategies for the acquisition of weak GNSS signals must be considered. The integration time extension was exploited at acquisition-level,

Table 2: Number of GNSS satellites signals acquired versus distance from Earth processing simulated RF samples.

T_{coh} (ms)	30RE	45RE	60RE	61RE MSO
1	1	0	0	0
10	4	3	4	2

(a) GPS (L1 C/A)

T_{coh} (ms)	30RE	45RE	60RE	61RE MSO
4	1	3	0	0
12	4	3	4	0

(b) Galileo E1C

leveraging a coherent and a non-coherent approach (Spilker Jr et al., 1996). As shown in Tables 2a and 2b, we were not able to acquire any satellite when the coherent integration time was equal to the code period. Therefore a value of coherent time extension of 10 ms and 12 ms were chosen for GPS and Galileo, respectively, setting the number of non coherent accumulations equal to 6 (Spilker Jr et al., 1996). This setup enables signal acquisition with snapshots of less than 100 ms in the majority of cases, without resorting to advanced weak signal acquisition techniques such as Doppler compensation, but it is important to underline that for 45RE and 60RE we had more than one snapshot available. For a thorough characterization of the acquisition performance under this circumstances, the reader can refer to (Nardin et al., 2022b).

After characterizing the acquisition, the tracking parameters of the receiver were tuned according to the analyses' outcomes in Section IV.1. The resulting parameters of the software receiver are summarized in Table 3. Varying parameters are reported in italics. They were tested to find the best set of values for tracking results. The best set depends on the characteristics of the signal, hence it must be found specifically for each dataset. A PLI threshold of 0.766 has been set, which corresponds to a

Table 3: Software receiver configuration. Varying parameters are highlighted in italics.

Parameter	GPS	Galileo
Tcoh Acquisition	10 ms	12 ms
non-coherent accumulations	6	6
Doppler bin size	50 Hz	100 Hz
False Alarm Probability	1e-3	1e-3
DLL Bandwidth	10 Hz	10 Hz
PLL order	3	3
PLI threshold	0.766	0.766
DLL Correlator Spacing	0.2-1 chip	0.2-1 chip
Tcoh Tracking	4-20 ms	4-20 ms
PLL bandwidth	1-10 Hz	1-10 Hz
FLL duration	0-400 ms	0-400 ms

phase error of 20°. Such a value is based on tracking results obtained during the preliminary analysis. A time to lock (TTL) definition is proposed based on the PLI computation. The TTL is defined as the first time at which a *lock condition* is achieved, meaning that the tracking loop is able to follow the phase and code delay of the incoming signal. The decision logic described in Section II.2 was designed and implemented as depicted in Figure 2, by assessing its validity through preliminary experiments. For the purpose of this work, the TTL is computed with $M = 5$. In other words, the lock is declared when the PLI is greater than the PLI threshold for five consecutive tracking loops and the time of convergence is evaluated at the first of these loops. A sequence of values above the threshold is used to increase the lock declaration robustness coping with the fluctuations of PLI values, also according to the considerations of Section II.2. When the FLL-based initialization is present, the FLL time is accounted for in the final TTL, adding it to the PLI-based evaluation. After setting the parameters, the simulated data (simulated RF samples and N-FUELS samples) are entirely processed with the tuned software receiver to assess the TTL performance. Results are reported in Section IV.2.

3. Monte Carlo Simulations Setup

The second part of the experiments is devoted to a Monte Carlo simulation performed to investigate the impact of the signal parameters on the tracking performances. The parameters analyzed are the sampling frequency and the number of quantization bits of the signals. The impact of these parameters on our analysis can be essential, since there is a direct dependence with the data volume of the generated IQS. In fact, the larger the value of the sampling frequency the larger is the data volume of the snapshot for a fixed signal duration, since more samples are saved. An analogous discussion can be repeated for the quantization

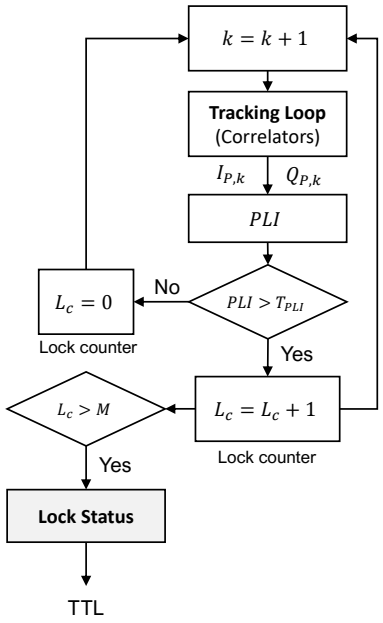

Figure 2: Logic for the declaration of successful tracking lock.

bits. If the number of quantization bits increases, the IQS data volume increases as well. A practical example of the mentioned trend is depicted by Figure 3 for a specific case of snapshot duration of 300 ms. The IQS data volume is bounded by the payload

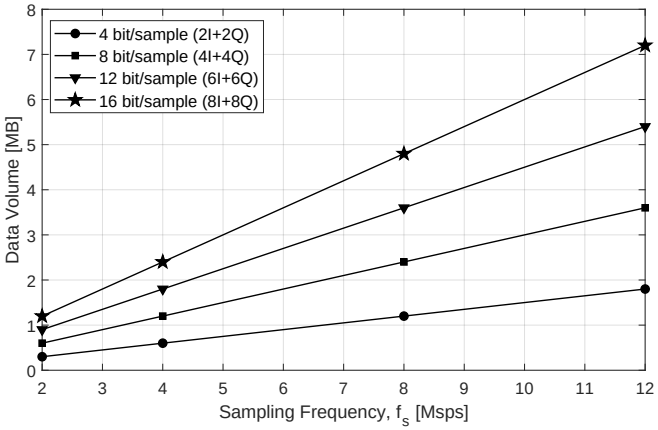

Figure 3: Data volume of a 300 ms IQS snapshot versus suitable L1 sampling frequency for different amount of quantization bits.

constraints set by the mission design, thus it should be reduced as much as possible to increase the snapshot time-duration. The aim of the analysis in Section IV.3 is to investigate the trade-off between the resolution and the length of the signal, to understand if it is convenient to have a signal with more samples per second and a higher quantization depth or a signal that spans over a longer time window. The flexibility provided in the generation of the N-FUELS samples allows us to explore this trade-off.

IV. RESULTS AND DISCUSSION

The first part of this section reports the results of the preliminary parametrical analysis intended for a fine-tuning of the software receiver. The following part is then dedicated to analyze and process the simulated RF samples obtained from the LuGRE front-end in a realistic scenario. Given a fixed duration of the snapshots, the aim of the analysis is to understand the achievable performance. In the final subsection a comprehensive Monte Carlo simulation investigates the impact of front-end parameters.

This allows to define an acceptable and reasonable value of the size of the snapshots taking into account the mission design limitations.

1. Parametric Analysis: Software Receiver Tuning

a) PLL bandwidth

The mission scenario will be characterised by unfavourable C/N_0 and possibly dynamic stress. Two competing challenges with respect to the PLL bandwidth, which must be large enough to follow variable dynamics and narrow enough to limit the amount of noise in the loop. A preliminary analysis showed that a 10 Hz bandwidth should suffice for C/N_0 above 24 dB-Hz. For weaker signal reception conditions, a narrower bandwidth should be enforced or high-sensitivity techniques must be put in place (Domínguez et al., 2016; Musumeci et al., 2016b; Van Diggelen, 2020). Our results showed a successfull lock under mission dynamics also for a PLL bandwidth of 1 Hz in some cases. A varying PLL bandwidth between 1 and 10 Hz has been used in the following analyses to provide the best results.

b) Integration time

A simulation with varying C/N_0 ratios is suggested as a method for locating an appropriate value for the integration time. The carrier loop bandwidth is kept constant at 10 Hz, and integration times of 1 ms and 20 ms are tested for values of C/N_0 ranging from 24 to 38 dB-Hz. As can be seen in Table 4, for values of C/N_0 greater than or equal to 30 dB-Hz, we are able to track the most powerful satellite with either value of integration time. However, an integration time of 1 ms is insufficient to work at C/N_0 values lower than 30 dB-Hz. This is due to the fact that shorter values of integration result in more noisy estimation. Therefore, at low C/N_0 values, an integration time of 1 ms is not enough to make the tracking to converge. Conversely, with an integration time of 20 ms, we are able to track the signal to a C/N_0 as low as 24 dB-Hz. A long integration time makes the tracking less robust against high-dynamics. However, for the addressed scenario, an integration time of 20 ms is considered as an acceptable value to trade robustness to dynamics for tracking capabilities at low C/N_0.

Table 4: Tracked GPS L1 C/A signals for different C/N_0 with and without time extension.

Parameter		C/N_0 (dB/Hz)						
T_{coh}	B_{PLL}	24	26	28	30	32	35	37
1 ms	1 Hz				•	•	•	•
	10 Hz							
20 ms	1 Hz	•	•	•	•	•	•	•
	10 Hz		•	•	•	•	•	•

c) Early-Late spacing

During our investigation, we examined whether or not there would be a positive impact if the spacing between the early and late components of the DLL (Kaplan and Hegarty, 2017) was made smaller in a space scenario. The simulation was performed on the simulated RF samples at 45RE and 60RE. We observed that in both situations no gain in terms of tracking performances was identifiable. The spacing reduction was neither able to make the tracking to converge when not locked, nor able to reduce the time to reach the tracking convergence. The resulting TTL is unchanged and the only beneficial effect observed was a less noisy DLL outcome. Our goal is to minimize the TTL value, hence the value of the E-L spacing does not have significant impact on our analysis.

d) FLL aid

Various simulations were performed in different conditions: using only the PLL, or using the FLL to initialize the PLL, varying the FLL duration to identify a profitable value. Figure 4 shows the comparison of two tracking outputs, with and without the FLL, at a distance of 60 RE. The plots depict the changes in the values of correlator outputs $Q_{P,k}, I_{P,k}$, with respect to time (right plots), or in a scatter diagram (left plots). The signal under test was GPS L1 C/A, extracted from simulated RF samples. We can notice that the lock condition is not satisfied when the FLL is not employed. The points of the scatter plot show a rotating trend. This is the typical situation where the phase rotates due to a not accurate starting frequency value that can be improved by means of the FLL assistance. Indeed, by using 300 ms of FLL aid, the lock is achieved after 100 ms with an overall TTL of 400 ms. The scatter points show either values around ($I_{P,k} = 1, Q_{P,k} = 0$) or ($I_{P,k} = -1, Q_{P,k} = 0$), which is correct since the signal contains the navigation message. Note that also the FLL has its own bandwidth that is fixed to 15 Hz following analogous considerations discussed during the design of the PLL bandwidth. With this tracking architecture, a brief assistance of FLL is recommended in any situation to process the IQS. Its duration could be fixed in post-processing for each individual signal, taking into account the Doppler dynamics and the C/N_0.

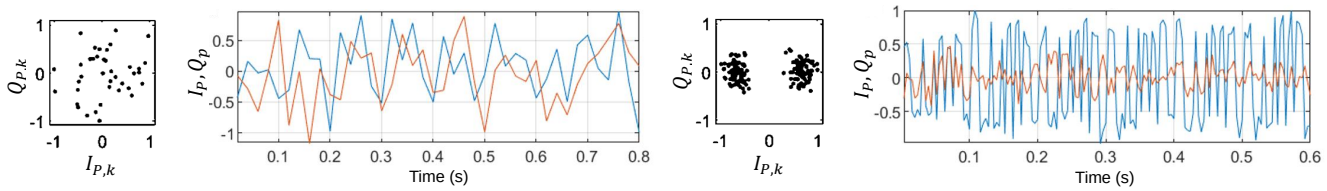

(a) No FLL-based initialization

(b) FLL-based initialization for 300 ms

Figure 4: Comparison of the tracking results of a 1 s GPS L1 C/A signal at 60RE for different FLL durations.

Table 5: TTL values reducing the Doppler frequency bins.

Doppler step (Hz)	TTL (ms)
50	500
10	150

(a) GPS L1 C/A

Doppler step (Hz)	TTL (ms)
100	120
20	120

(b) Galileo E1c

e) Doppler bin size

Alongside with the use of FLL, also a finer resolution of the acquisition process could help improving the tracking estimation of the carrier and, ultimately, the TTL. This parameter does not affect directly the tracking output, but it could allow to start from a more precise value of the estimated Doppler shift fed to the tracking stage by the acquisition. In particular, the size of the Doppler bin in the acquisition search space could reduce the TTL at the cost of a longer processing time. Starting from a better estimation, the time-length of the signal needed at the tracking stage to converge to a frequency and phase lock condition is reduced. Two different experiments were carried out using simulated RF samples, one for GPS L1 C/A and the other for Galileo E1C. Tables 5a and 5b summarize the results, reporting the TTL values obtained during the simulations. We can observe that for the GPS signal, the increase of resolution on the Doppler gives a better initialising frequency to the tracking stage so that the TTL is reduced from 500 ms, with a resolution of 50 Hz, to 150 ms with a resolution of 10 Hz. However, for Galileo E1C the tracking outputs lead to identical TTL values for both cases. In this particular situation, the Doppler frequency bins reduction does not provide any advantage, although it cannot worsen the Doppler estimation of the acquisition stage. Our analysis showed that an increase of Doppler resolution may be beneficial in some cases and could be generally used as an effective means of TTL performance improvement.

2. Realistic Scenario: RF Signals and LuGRE Front-end

The previous results enabled to narrow the range of suitable parameters of the GNSS software receiver settings, illustrated in Table 3. Spanning among them to find the best conditions, we were able to observe the performance summarized in Table 6, which reports aggregated statistics on the simulated RF samples modelled for the LuGRE mission. The maximum, the mean and the minimum value of TTL are reported. The results are based on 7 out 8 signals (see Table 1) for which a locked condition was declared (3 for GPS and 4 for Galileo).

The results indicate that with a signal duration of 200 ms, few signals can be tracked and if this value grows to 400 ms, the lock is achieved for a larger number of signals. We can suppose that an order of magnitude of 300-400 ms of snapshot duration is enough to track at least one satellite in the majority of cases. It is important to underline that this duration allows the initial assistance of the FLL that is crucial in most of the situations to track the signals. By just employing a PLL, the number of locks obtained drops from 7 to 1. Further post-processing analyses can be performed trying to improve the results, even modifying the tracking architecture to better fit the space scenario. Furthermore, an external aiding such as the orbital filter can be used to retrieve information about the Doppler and reduce or even remove the initial assistance of the FLL, leading to a further improvement.

3. Statistical Analysis of Locking Performance

a) Impact of the Sampling frequency

The first analysis focuses on comprehending how the sampling process influences tracking performance. As mentioned in Section III.3, a larger sampling frequency means a bigger data volume and, therefore, a smaller signal duration available on ground. It is therefore quite useful to analyze the tracking performance varying the value of the sampling frequency and trying to approach an optimal value for the mission. The values of the sampling frequency tested are 4, 8 and 12 Msps, while the number

Table 6: TTL values statistics of simulated RF signals and LuGRE front-end

Parameter	Value (ms)
Minimum TTL	80
Maximum TTL	500
Mean TTL	335

of quantization bits is fixed to 8, based on the characteristic of the simulated RF samples dataset. A Monte Carlo simulation is performed for each value of frequency and for different points on the receiver orbits: at 45 RE and 60 RE. During the experiments the duration of the FLL was fixed to 200 ms. The outputs of the simulations are the mean TTL and the percentages of lock (POL), both key quantities to characterize the processing of the tracking stage from a statistical point of view. The mean TTL is obtained averaging the values of the TTL for each realization only when lock is achieved, otherwise no significant value of TTL can be computed. The POL is the normalized number of Monte Carlo realizations that achieve the lock condition. The total number of Monte Carlo simulations is fixed to 1000. This value was found to be reasonable after monitoring the empirical convergence of the variable at stake. Indeed, Figure 5 depicts the mean TTL during the experiment versus the number of lock achieved. We can note that just after 200 locks the mean approaches stability since no significant fluctuations are present. We can conclude that the number of iterations is enough to get a stable convergence of the mean. It is important to underline that the number of locks does not coincide with the total number of iterations since in some cases the tracking cannot achieve the lock condition. To this purpose, the POL variable is considered.

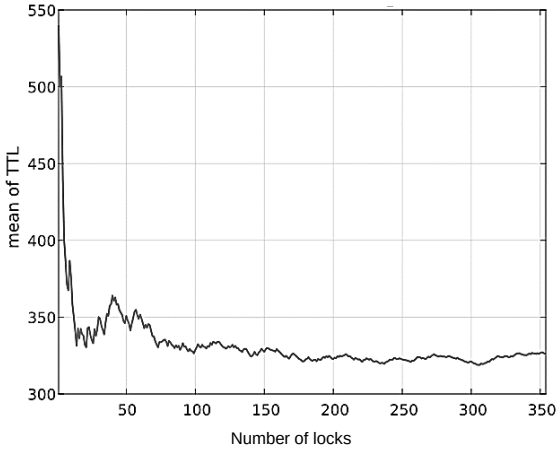

Figure 5: Evolution of the mean TTL during the simulation. The x-axis shows the progressive number of locks during the simulation.

As it can be expected, the results shows that the mean TTL decreases with the sampling frequency while the POL increases, although at a relatively small rate in both cases (Figure 6 and Figure 7). In other words, we have a performance gain by increasing the sampling frequency and this holds for both the mean TTL and the POL. However, as mentioned before, a higher sampling frequency means a lower duration of a fixed data-size snapshot. Therefore, a trade-off arises between the gain obtained in terms of tracking performances and the reduction of data time-length. For example, if the sampling frequency reduces from 8 to 4 Msps, the data volume decreases from 2.4 MB to 1.2 MB (fixing the IQS duration to 300 ms). However, the tracking performances get worse, demanding a higher TTL on average. For instance, considering the case of Galileo at 60RE (Figure 7), the POL drops from 30% to 24% and the mean TTL increases from 300 ms to 345 ms. Therefore, the design choice could be either having an IQS duration of 300 ms with 8 Msps of sampling frequency corresponding to a data volume of 2.4 MB or an IQS duration of 400 ms with 4 Msps which corresponds to a data volume of 2 MB. Based on this consideration the best choice seems to be the second one, with 4 Msps, since a 400 ms snapshot can better accommodate a mean TTL of about 340 ms (i.e. the mean TTL for Galileo E1C sampled at 4 Msps, see Figure 7b). On the contrary, a 300 ms snapshot available after a 8 Msps sampling cannot allow to track all the signals whose TTL would be above the mean TTL of 300 ms. Moreover, with a 2 MB data volume we can further increase the snapshot duration to reach 2.4 MB or save memory and transmission time during the data collection. Indeed the POL and TTL gets worse with a lower sampling frequency,

At shorter distances from GNSSs orbits (Figure 6) we have a larger POL, hence higher chances to track a signal, although it is worth noticing that the mean TTL performance of the locked realizations are only slightly affected. This suggests that, albeit

we might have more chances to achieve lock, better mean TTL performances are hard to achieve in these conditions and with the current architecture.

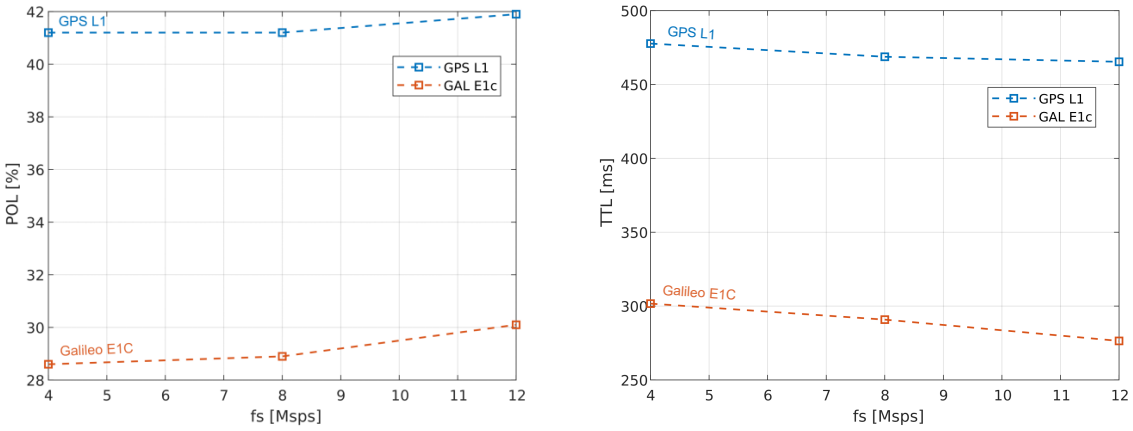

(a) POL versus sampling frequency

(b) TTL versus sampling frequency

Figure 6: Sampling frequency analysis, 45RE.

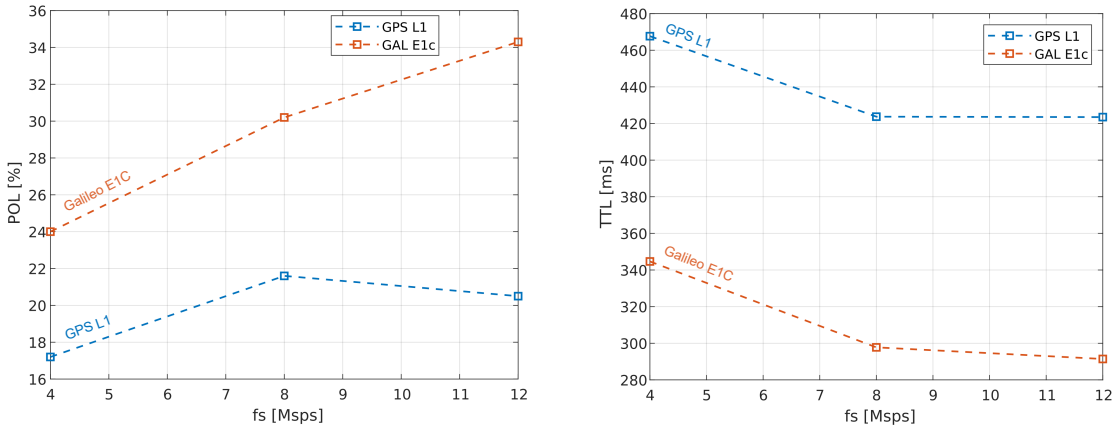

(a) POL versus sampling frequency

(b) TTL versus sampling frequency

Figure 7: Sampling frequency analysis, 60RE.

b) Impact of the number of quantization bits

An analogue analysis is repeated by testing the impact of the number of quantization bits on the tracking performances, again in terms of POL and mean TTL. To this purpose, during this experiment the number of quantization bits antecedently fixed to 8, now takes the values of 4, 6, and 8 bits, while the sampling frequency is fixed to 8 Msps. A Monte Carlo approach is proposed using a number of simulations equal to 1000 and testing simulated signals (N-FUELS samples) as received at 45 RE and 60 RE from Earth. The FLL duration was fixed to 200 ms. Differently from the previous outcomes, the following results do not show a clear trend varying the number of quantization bits, rather, the mean TTL and POL seems to be not affected by this change, being basically constant for different number of quantization bits, as shown in Figure 8, for the 45 RE case. Similar observations were done for the 60 RE case, whose results are omitted for the sake of brevity. This suggests to reduce as much as possible the number of quantization bits as they do not bring relevant performance gain for the investigated metrics. For plain tracking purposes and with the current receiver architecture, there are no reasons to use a large quantization depth. On the other hand, by reducing the number of quantization bits, the data volume is reduced as well, granting the possibility to save memory that can be crucial to face the stringent constraints on the data storage during the mission or exploiting the limited downlink transmission bandwidth to convey to the ground a longer GNSS signal snapshot.

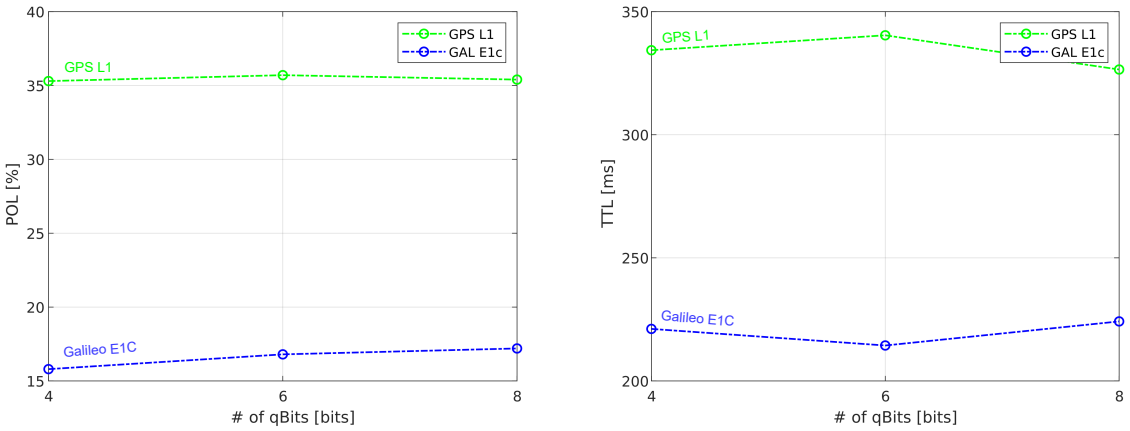

(a) POL versus no. of quantization bits

(b) TTL versus no. of quantization bits

Figure 8: Samples of POL (a) and TTL(b) analysis varying the quantization bits at 45RE.

c) Considerations on IQS duration

After discussing the impact of the digitized samples parameters, additional considerations about snapshots duration should be done. To this purpose, Figure 9 and Figure 10 describe, with histograms, the distribution of TTL during the single Monte Carlo experiment and the corresponding cumulative POL. The yellow line indicates, as a reference term, the POL for a given snapshot duration of 300 ms. Focusing on Figure 9 to give an example, if we choose a snapshot duration of 300 ms, then we will have 28% probability to achieve the tracking lock at 45RE on GPS L1 C/A, while if we are able to record longer signals, up to 500 ms, the chances to track the GPS signal grows to 38%.

We can notice from the figures that some differences emerges on the distribution of the TTL between GPS and Galileo cases. To be more specific, the TTL distribution of GPS appears more widespread, suggesting that the TTL value is characterized by a higher variance. Conversely, the TTL values of Galileo are more concentrated around one single value, showing a lower variance. It is worth mentioning that the results were obtained with an FLL duration set to 200 ms, so that the minimum TTL value obtainable is 200 ms. Moving from a distance of 45 RE to 60 RE the results get worse, as expected, since the signal is characterized by a higher noise level. For instance, the probability to achieve the lock with a duration of 400 ms drops from 36 % to 9 % in case of GPS signal. Similarly, the chances to track a Galileo signal reduces from 23 % to 16 % for a snapshot duration of 300 ms. However, the Galileo signal appears to be more robust against higher distances than GPS signal, since the impact on the POL is lighter. The reasons behind that needs to be searched both in the signal characteristics and in the specific processing architecture of our receiver. A further analysis needs to be done to properly answer the question.

Tables 7a and 7b report the probability to track at least one GNSS signal (GPS or Galileo) for different values of snapshot duration. The proposed probability is computed summing the probability to track a GPS satellite with a probability to track a Galileo satellite, since it represents the chance to track at least one signal belonging to one of the two constellations. The joint probability of the two events is then subtracted according to the union rule. If the two events are statistically independent, the probability of the intersection can be computed as the product between the probabilities of the two events. Under this simplifying assumption, the results indicate that with a time window ensuring to collect at least 300 ms of data, the possibility to achieve a successful tracking are 45 % at 45 RE and nearly 20 % at 60 RE. If the length of the snapshots collected is extended to 400 ms, the probabilities increase to 51 % and 30 % respectively. Conversely, if the snapshot duration available is in the order of 250 ms, the chances drop to 28 % at 45 RE and only 4 % at 60 RE. This strongly suggests the need to collect at least 300 ms of data to have reasonable chances to achieve a successful tracking. This is also supported by the fact that an FLL duration of 200 ms seems to be the minimum value granting the possibility to pull aside the signal. It is worth stressing that such investigated snapshot durations will mostly characterize the data collection during the transit phase, where a limited transmission capacity is granted. On the moon surface, at around 60 RE, snapshot collections of about 2500 ms will be likely available at the ground.

It is important to underline that these are just preliminary results, obtained taking just one set of the receiver parameters for each realization. Therefore, they might represent an unfavorable case given that when the real collected data will be available, the flexibility of the software receiver can be leveraged to boost the processing effectiveness. Indeed, for each available snapshot under test, a wide range of receiver architectures and parameters can be tested. The presented results can be useful during the design of the IQS time window of the mission. The best trade-off must be found taking into account the mentioned considerations and the mission limitations on data storage and transmission.

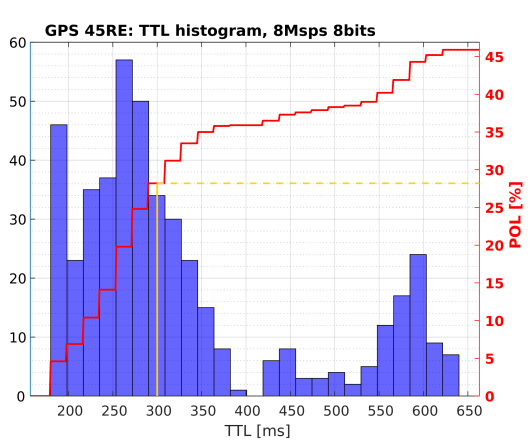

(a) GPS L1 C/A

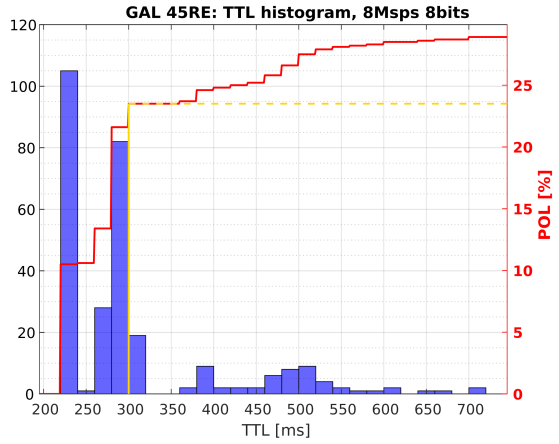

(b) Galileo E1c

Figure 9: TTL histogram and corresponding cumulative POL, 8 Msps of sampling frequency and 8 bits as number of quantization bits, 45RE.

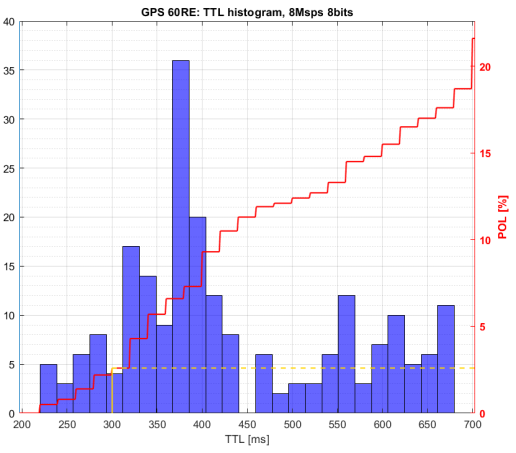

(a) GPS L1 C/A

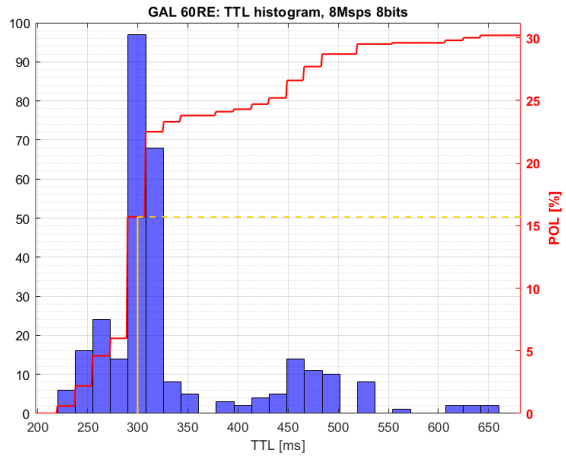

(b) Galileo E1c

Figure 10: TTL histogram and corresponding cumulative POL, 8 Msps of sampling frequency and 8 bits as number of quantization bits, 60RE.

V. CONCLUSIONS

The LuGRE mission, scheduled in 2024, will attempt to retrieve GNSS signal samples and navigation data on its way to the Moon to demonstrate GNSS usability beyond the current record of 29 RE. By assuming a limited on-board storage capability, as well as limited downlink opportunities, this work analyzed the tracking performance of simulated IQS signals within the LuGRE framework to determine a minimum snapshot duration to be returned to the ground segment for scientific investigations. These signals have been processed through a GNSS software receiver that leverages specific high-sensitivity solutions to guarantee effective signal acquisition and tracking in low C/N_0 conditions. Monte Carlo simulations were executed for a classical tracking loop to estimate the probabilities to successfully track a signal snapshot of a given duration. This approach allowed us to investigate the impact of the sampling frequency and of the number of quantization bits on the tracking performances on a statistical basis. The results show that the performance degrades by reducing the sampling frequency, while the impact of quantization bits reduction is only slightly relevant. Hence, reducing the latter, longer snapshot captures will be possible throughout the mission with a negligible impact on both acquisition and tracking performance. Our investigation highlights that 400 ms of recorded snapshots are a valuable trade-off to guarantee a successful tracking in about 51 % and 30 % of cases at 45 RE and 60 RE, respectively. Below this threshold, the chances to track GNSS signals dramatically drop. The accomplished results and considerations can be exploited during the design of the concept of operations for capturing IQS windows during the LuGRE mission.

Table 7: Probability to track GNSS signals varying the IQS duration.

IQS snapshot duration	Signal tracking probability
250 ms	$\simeq$ 28 %
300 ms	$\simeq$ 45 %
400 ms	$\simeq$ 51 %
500 ms	$\simeq$ 55 %

(a) 45RE

IQS snapshot duration	Signal tracking probability
250 ms	$\simeq$ 4 %
300 ms	$\simeq$ 18 %
400 ms	$\simeq$ 30 %
500 ms	$\simeq$ 36 %

(b) 60RE

ACKNOWLEDGEMENTS

This study was funded within the contract n. 2021-26-HH.0 ASI/Politecnico di Torino "Attività di R&S inerente alla Navigazione GNSS nello Space volume Terra/Luna nell'ambito del Lunar GNSS Receiver Experiment". The authors would like to thank Qascom s.r.l. for providing simulated data. A. Minetto acknowledges funding from the research contract no. 32-G-13427-5 DM 1062/2021 sustained by the Programma Operativo Nazionale (PON) Ricerca e Innovazione of Italian Ministry of University and Research.

REFERENCES

Baird, D. (2019). Record-breaking satellite advances NASA's exploration of high-altitude GPS. *www.nasa.gov*. Accessed on: Nov. 23, 2022.

Baird, D. (2021). NASA explores upper limits of global navigation systems for artemis. *www.nasa.gov*. Accessed on: Nov. 23, 2022.

Borio, D. and Gioia, C. (2023). Reconstructing GNSS meta-signal observations using sideband measurements. *NAVIGATION: Journal of the Institute of Navigation*, 70(1).

Capuano, V. (2015). GNSS-based orbital filter for Earth Moon transfer orbits. *Journal of Navigation*.

Capuano, V., Blunt, P., Botteron, C., Tian, J., Leclère, J., Wang, Y., Basile, F., and Farine, P.-A. (2016). Standalone GPS L1 C/A receiver for lunar missions. *Sensors*, 16:347.

Delépaut, A., Minetto, A., Dovis, F., Melman, F., Giordano, P., and Ventura-Traveset, J. (2022). Enhanced GNSS-based positioning in space exploiting inter-spacecraft cooperation. In *Proceedings of the 2022 International Technical Meeting of The Institute of Navigation*, pages 530–544.

Delépaut, A., Giordano, P., Ventura-Traveset, J., Blonski, D., Schönfeldt, M., Schoonejans, P., Aziz, S., and Walker, R. (2020). Use of GNSS for lunar missions and plans for lunar in-orbit development. *Advances in Space Research*, 66(12):2739–2756. Scientific and Fundamental Aspects of GNSS - Part 1.

Domínguez, E., Pousinho, A., Boto, P., Gómez-Casco, D., Locubiche-Serra, S., Seco-Granados, G., López-Salcedo, J., Fragner, H., Zangerl, F., Peña, O., et al. (2016). Performance evaluation of high sensitivity GNSS techniques in indoor, urban and space environments. In *Proceedings of the 29th International Technical Meeting of the Satellite Division of The Institute of Navigation (ION GNSS+ 2016)*, pages 373–393.

Dovis, F. and Ta, T. H. (2012). High sensitivity techniques for GNSS signal acquisition. In Jin, S., editor, *Global Navigation Satellite Systems*, chapter 1. IntechOpen, Rijeka.

Falletti, E., Margaria, D., Nicola, M., Povero, G., and Gamba, M. T. (2013). N-FUELS and SOPRANO: Educational tools for simulation, analysis and processing of satellite navigation signals. In *2013 IEEE Frontiers in Education Conference (FIE)*, pages 303–308.

Fernández-Hernández, I. and Borre, K. (2016). Snapshot positioning without initial information. *GPS solutions*, 20(4):605–616.

Franzese, V., Lizia, P. D., and Topputo, F. (2018). Autonomous optical navigation for LUMIO mission. *2018 Space Flight Mechanics Meeting*.

ISECG, I. S. E. C. G. (2018). The Global Exploration Roadmap. Technical report, International Space Exploration Coordination Group (ISECG).

Israel, D. J., Mauldin, K. D., Roberts, C. J., Mitchell, J. W., Pulkkinen, A. A., Cooper, L. V. D., Johnson, M. A., Christe,

S. D., and Gramling, C. J. (2020). LunaNet: a flexible and extensible lunar exploration communications and navigation infrastructure. In *2020 IEEE Aerospace Conference*, pages 1–14.

Kaplan, E. D. and Hegarty, C. (2017). *Understanding GPS/GNSS: Principles and applications*. Artech house.

Minetto, A., Dovis, F., Nardin, A., Vouch, O., Impresario, G., and Musmeci, M. (2022). Analysis of GNSS data at the Moon for the LuGRE project. In *2022 IEEE 9th International Workshop on Metrology for AeroSpace (MetroAeroSpace)*, pages 134–139.

Musumeci, L., Dovis, F., Silva, J., Silva, P. F., and Lopes, H. (2016a). Design of a high sensitivity GNSS receiver for lunar missions. *Advances in Space Research*, 57.

Musumeci, L., Dovis, F., Silva, J. S., da Silva, P. F., and Lopes, H. D. (2016b). Design of a high sensitivity GNSS receiver for lunar missions. *Advances in Space Research*, 57(11):2285–2313.

Nardin, A., Dovis, F., and Fraire, J. A. (2020). Empowering the tracking performance of LEO PNT by means of meta-signals. In *2020 IEEE International Conference on Wireless for Space and Extreme Environments (WiSEE)*, pages 153–158.

Nardin, A., Dovis, F., and Fraire, J. A. (2021). Empowering the tracking performance of LEO-based positioning by means of meta-signals. *IEEE Journal of Radio Frequency Identification*, 5(3):244–253.

Nardin, A., Fraire, J. A., and Dovis, F. (2022a). Contact plan design for GNSS constellations: A case study with optical intersatellite links. *IEEE Transactions on Aerospace and Electronic Systems*, 58(3):1981–1995.

Nardin, A., Minetto, A., Vouch, O., Mariani, M., and Dovis, F. (2022b). Snapshot acquisition of GNSS signals in space: a case study at lunar distances. In *Proceedings of the 35th International Technical Meeting of the Satellite Division of The Institute of Navigation (ION GNSS+ 2022)*, pages 3603 – 3617, Denver, Colorado.

Parker, J. J. K., Dovis, F., Anderson, B., Ansalone, L., Ashman, B., Bauer, F. H., D'Amore, G., Facchinetti, C., Fantinato, S., Impresario, G., McKim, S. A., Miotti, E., Miller, J. J., Musmeci, M., Pozzobon, O., Schlenker, L., Tuozzi, A., and Valencia, L. (2022). The Lunar GNSS Receiver Experiment (LuGRE). In *Proceedings of the 2022 International Technical Meeting of The Institute of Navigation*, pages 420–437, Long Beach, California.

Savas, C., Falco, G., and Dovis, F. (2021). A comparative performance analysis of GPS L1 C/A, L5 acquisition and tracking stages under polar and equatorial scintillations. *IEEE Transactions on Aerospace and Electronic Systems*, 57(1):227–244.

Silva, P., Lopes, H., Peres, T., Silva, J., Dovis, F., Musumeci, L., Serant, D., Calmettes, T., Pessina, I., and Perello, J. (2013). Weak GNSS signal navigation to the Moon. In *Proceedings of the 26th International Technical Meeting of the Satellite Division of The Institute of Navigation (ION GNSS+ 2013)*, volume 4, pages 3357–3367, Nashville, TN.

Spilker Jr, J. J., Axelrad, P., Parkinson, B. W., and Enge, P. (1996). *Global positioning system: theory and applications, volume I*. American Institute of Aeronautics and Astronautics.

Teunissen, P. J. G. and Montenbruck, O. (2017). *Springer handbook of global navigation satellite systems*, volume 10. Springer.

Thornton, C. and Border, J. (2003). *Radiometric Tracking Techniques for Deep-Space Navigation*, volume 2. John Wiley & Sons, Ltd.

Van Diggelen, F. (2020). High-sensitivity GNSS. *Position, navigation, and timing technologies in the 21st century: Integrated satellite navigation, sensor systems, and civil applications*, 1:445–479.

Williams, J. G. and Dickey, J. O. (2002). Lunar geophysics, geodesy, and dynamics. In *13th International Workshop on Laser Ranging*, Goddard Space Flight Center.

Winternitz, L. B., Bamford, W. A., Price, S. R., Carpenter, J. R., Long, A. C., and Farahmand, M. (2017). Global positioning system navigation above 76,000 km for NASA's magnetospheric multiscale mission. *NAVIGATION*, 64(2):289–300.

Xiaolin, N. et al. (2018). Pulsar navigation using time of arrival (TOA) and time differential toa (TDTOA). *Acta Astronautica*, 142:57–63.

Yang, R., Ling, K.-V., Poh, E.-K., and Morton, Y. (2017). Generalized GNSS signal carrier tracking: Part I—modeling and analysis. *IEEE Transactions on Aerospace and Electronic Systems*, 53(4):1781–1797.